Journal of Solid State Chemistry 218 (2014) 213–220

Contents lists available at ScienceDirect

Journal of Solid State Chemistry

journal homepage: www.elsevier.com/locate/jssc

Hierarchical Na-doped cubic ZrO_2 synthesis by a simple hydrothermal route and its application in biodiesel production

Hugo A. Lara-García, Issis C. Romero-Ibarra, Heriberto Pfeiffer *

Instituto de Investigaciones en Materiales, Universidad Nacional Autónoma de México. Circuito exterior s/n, Cd. Universitaria, Coyoacán CP 04510, México DF, Mexico

ARTICLE INFO

Article history:
Received 7 April 2014
Received in revised form
30 May 2014
Accepted 24 June 2014
Available online 1 July 2014

Keywords:
Hydrothermal synthesis
Cubic ZrO_2
Nanoparticles
Biodiesel
Zirconia

ABSTRACT

Hierarchical growth of cubic ZrO_2 phase was successfully synthesized via a simple hydrothermal process in the presence of different surfactants (cationic, non-ionic and anionic) and sodium hydroxide. The structural and microstructural characterizations of different ZrO_2 powders were performed using various techniques, such as X-ray diffraction, transmission electron microscopy, N_2 adsorption–desorption, scanning electron microscopy and infrared. Results indicated that sodium addition stabilized the cubic ZrO_2 phase by a Na-doping process, independently of the surfactant used. In contrast, microstructural characteristics varied as a function of the surfactant and sodium presence. In addition, water vapor (H_2O) and carbon dioxide (CO_2) sorption properties were evaluated on ZrO_2 samples. Results evidenced that sample surface reactivity changed as a function of the sodium content. Finally, this surface reactivity was evaluated on the biodiesel transesterification reaction using the different synthesized samples, obtaining yields of 93%.

1. Introduction

Zirconia (ZrO_2) is extensively studied and used in different applications such as thermal barrier coatings, solid oxide ion conductor, optical and electric application and as catalyst, among others [1–8]. Actually, ZrO_2 can be used in many applications due to its possible structural changes between monoclinic, tetragonal and cubic phases. Of course, the cubic and tetragonal ZrO_2 stabilization depends on different mechanisms such as particle size, constrainment and doping [4,9–15]. As an example of these structural variations, Näfe and Karpukhina studied the Na_2ZrO_3–ZrO_2 system, finding out that Na-doped cubic ZrO_2 phase is thermally stable [9].

Zirconia has been used as support or associated with other oxides in catalytic applications. There have been some studies on the usage of ZrO_2 as a solid catalyst for transesterification reactions [16–17]. This reaction is the key step in biodiesel production. Li et al. reported a solid base catalyst prepared by the sodium potassium tartrate doped zirconia as catalyst in biodiesel production via the transesterification reaction. However, in most catalytic investigations the zirconia is used as a support [16].

On the other hand, there are several emerging synthetic approaches to obtain useful advanced porous ceramics, at relatively low temperatures [18–22], with different textural and morphological characteristics that can be valuable and expand the scope of novel applications. In addition, it seems that the use of surfactants added in different routes of chemical synthesis, which not only affect the crystallization of single particles, but also influence the formation of complex microstructures [10,18,23–28]. These techniques include coprecipitation, sol–gel, combustion and surfactant-assisted solvothermal and hydrothermal approaches, among others. Among the chemical preparation methods, hydrothermal route has been recognized as energy and time saver with faster kinetics of crystallization than classic co-precipitation or sol–gel methods [29].

Therefore, the present work aimed the systematic study of a simple hydrothermal synthesis route of Na-doped cubic ZrO_2 phase, using different surfactants (cationic, non-ionic and anionic), to establish the effect of the synthetic route on the structural, microstructural and chemical-surface characteristics of the resultant ZrO_2. To evaluate the superficial reactivity various N_2–H_2O and CO_2–H_2O thermogravimetric dynamic experiments were performed. Additionally, samples were evaluated as possible catalysts. Specifically, the biodiesel production via the transesterification reaction was performed.

2. Experimental procedure

Zirconium acetate ($Zr–(OCH_3)_4$, Aldrich) was selected as starting zirconium material. To modify the synthesis three reagents

* Corresponding author. Tel.: +52 55 5622 4627; fax; +52 55 5616 1371.
E-mail address: pfeiffer@iim.unam.mx (H. Pfeiffer).

http://dx.doi.org/10.1016/j.jssc.2014.06.040
0022-4596/

were used as surfactants varying ionic properties: cetyltrimethylammonium bromide (CTAB, 99%, from Aldrich, with cationic character), octylphenol ethylene oxide condensate (TRITON-114X, 99% from Aldrich, with non-ionic character) and sodium dodecylbenzene sulfate (SDBS, 80%, from Aldrich, with anionic character). Initially, a determined quantity of the selected surfactant and zirconium acetate were dissolved in an aqueous ethyl alcohol solution with an alcohol:water volume ratio of 30:70. In other cases, sodium hydroxide (NaOH 98.1%, from Baker) was added to the previously described solutions, with a Na:Zr molar ratio of 2:1. The amount of surfactant was estimated to be 25 times the critical micelle concentration value (cmc) at 25 °C, depending on each surfactant [30–32]. Each solution was stirred using an ultrasonic bath for 15 min to obtain a homogeneous solution. In a further step, the solutions were transferred into a Teflon-lined stainless steel autoclave vessel, filling it up to 80% of its total volume. Hydrothermal reactions were performed at 150 °C for 24 h, under autogenous pressure. The autoclave vessel was cooled to room temperature. Then, the products were filtered and washed several times with distilled water. Finally, resulting powders were heated at 500 °C for 3 h, to eliminate any surfactant residue. The calcinations process was performed in air atmosphere.

A diffractometer (Siemens D-5000) coupled to a cobalt anode X-ray tube was used to identify the phases obtained during the different hydrothermal syntheses. The different phases and materials were identified using the Joint Committee Powder Diffraction Standards (JCPDS) files. To confirm the crystalline ZrO_2 phases present in the samples a transmission electron microscope (JEOL JEM-1200EX) was used.

The microstructural characteristics of the ZrO_2 samples were determined via N_2 adsorption–desorption and scanning electron microscopy (SEM). For the N_2 adsorption–desorption experiments, the isotherms were acquired on a Bel-Japan Minisorp II at 77K using a multi-point technique. Samples were degassed at room temperature for 24 h under vacuum prior to analysis. Then, the SEM experiments were performed on a JEOL JMS-7600F.

To elucidate if the samples presented different superficial reactivity, due to the sodium presence, different N_2–H_2O and CO_2–H_2O thermogravimetric dynamic experiments were performed using a humidity-controlled thermobalance (TA Instruments, model Q5000SA) at 60 °C, varying the relative humidity (RH) from 0 to 80% and then from 80 to 0% at a rate of 0.5%/min. The experiments were performed using distilled water and two different carrier gases: nitrogen (N_2, Praxair grade 4.8) or carbon dioxide (CO_2, Praxair grade 3.0). The total gas flow rate used in the experiments was 100 mL/min and the RH percentages were automatically controlled by the Q5000SA instrument. Finally, some CO_2–H_2O products were analyzed by attenuated total reflectance infrared spectroscopy (ATR-FTIR) using a Alpha-Platinum spectrometer from Bruker.

In addition, the catalytic activity was analyzed by the biodiesel transesterification production. Biodiesel consists of fatty acid methyl esters (FAME) and it is produced in a transesterification reaction as depicted in reaction 1. This reaction shows the transesterifaction of a triglyceride (vegetable oil) using an alcohol in presence of a catalyst.

Transesterification reactions were performed in a 25 mL three-neck round-bottomed glass flask equipped with a mechanical stirrer, a reflux condenser and a thermometer. The following reagents were used as received: analytical grade methanol (Sigma-Aldrich, 99.9% purity), ethanol (HPLC grade, Sigma-Aldrich) and pure Soybean oil, Nutrioli brand NOM-051-SCFI-SSA12010 that was purchased from local food store (Mexico, D.F). Catalysts (3 wt% based on oil weight) were mixed with methanol and soybean oil. The batch reactions were performed with 30:1 methanol/soybean oil molar ratio. The temperature of mixture was kept at 65 °C by a water bath. After the 3 h reaction time, the samples were immediately quenched in an ice bath (~4 °C) to control the conversion rate, and the different phases were separated using centrifugation. The biodiesel sample was characterized using the following techniques; attenuated total reflectance infrared spectroscopy (ATR-FTIR) and gas chromatography coupled to a mass spectrometer (GC–MS). ATR-FTIR spectra were obtained with an Alpha-Platinum spectrometer, from Bruker. GC–MS was performed on a QP2010 SE SHIMADZU equipment (with a capillary column Rx 23–30; 30 m × 0.25 mm), to evaluate the conversion and selectivity of the product over the transesterification reactions. The temperature of the detector was 250 °C, the ion source was 200 °C and the column temperature was programmed from 100 to 270 °C with the heating rate of 20 °C/min. The mobile phase was ethanol HPLC and its retention time was observed at 1.7 min. The final helium flow rate was 0.9 mL/min, and the sample injection volume was 1 μL. All analyses were performed at room temperature. The yield of biodiesel was calculated by the following equation: yield = W(biodiesel)/W(oil), where W(biodiesel) is the weight of produced biodiesel and W(vegetable oil) is the weight of oil. Finally, the biodiesel density was estimated according to the ASTM-D1298 norm.

3. Results and discussion

Fig. 1 shows the XRD patterns of the ZrO_2 hydrothermal samples prepared with different surfactants. While the ZrO_2 samples prepared with CTAB or triton 114X showed a mixture of monoclinic and cubic or tetragonal ZrO_2 phases in different abundances, the SDBS sample only showed the formation of the cubic or tetragonal ZrO_2 phase. This technique did not allow distinguishing if the ZrO_2 phase was cubic or tetragonal. In any case, the cubic or tetragonal phase presence must be explained based on the following different concepts: The cubic or tetragonal ZrO_2 phase formed with SDBS surfactant may be produced as doped ZrO_2 phase. Sodium dodecyl benzene sulfate (SDBS) is an ionic compound, which has sodium cations that are dissolved in the hydrothermal system. Under these conditions Na-doped ZrO_2 must be produced favoring the cubic or tetragonal phase stabilization. In fact, these results are in good agreement with Näfe and Karpukhina [9], who reported the Na-modified cubic ZrO_2 phase. Therefore, the presence of sodium in the SDBS hydrothermal solution must had induce the homogeneous formation of the cubic or tetragonal Na-doped ZrO_2 phase instead of the monoclinic one.

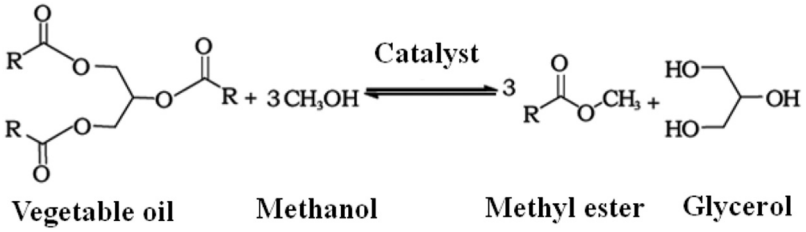

(1)

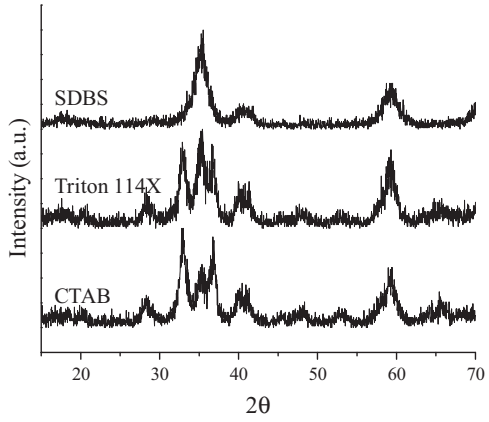

Fig. 1. XRD patterns of the ZrO_2 hydrothermal samples prepared with different surfactants; (A) CTAB, (B) triton 114X and (C) SDBS.

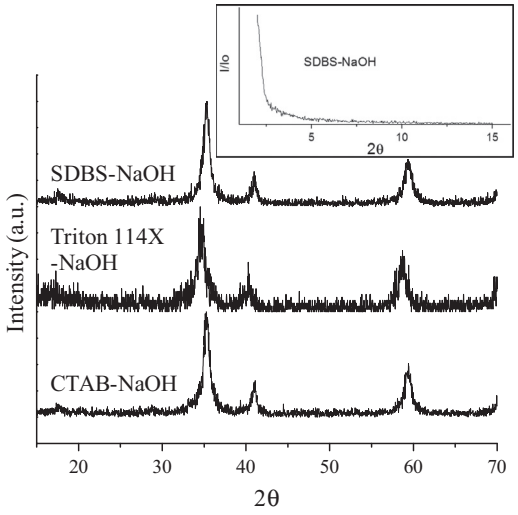

Fig. 2. XRD patterns of the ZrO_2 hydrothermal samples prepared in the presence of NaOH, using the following surfactants; (A) CTAB, (B) triton 114X and (C) SDBS. The inset shows the low angle XRD pattern (between 2° and 15°, 2θ range) of SDBS–NaOH.

On the other hand, the presence of the cubic or tetragonal ZrO_2 phase on the samples hydrothermally prepared with CTAB and triton 114X can not be explained in this way, as sodium was not present in those solutions. In these cases, the cubic or tetragonal ZrO_2 partial phase formation should be related to constrainment of the zirconia particles by the surrounding monoclinic ZrO_2 phase, on the basis of Garvie's hypothesis [1,11–14]. It has been reported that cubic or tetragonal ZrO_2 can be stabilized with small critical sizes ($\leq$ 50 nm), using different constrainment oxides such as SiO_2 or Al_2O_3 [1,11–12]. To corroborate this hypothesis different experiments were performed. First, the synthesized ZrO_2 samples using the three different surfactants were re-synthesized, but in this new synthesis sodium hydroxide (NaOH) was added as sodium source. As it would be expected, the XRD patterns of the ZrO_2 samples prepared with CTAB or triton 114X (Fig. 2) fitted to the cubic or tetragonal ZrO_2 phase, as the SDBS containing sample. These results confirmed that sodium ions induced the Na-doped cubic or tetragonal ZrO_2 phase formation. Additionally, the inset in Fig. 2 shows the low XRD angle pattern between 2° and 15° for the SDBS with NaOH. Then, there was not observed the formation of any ordered mesoporous structure. Similar results were obtained for all samples.

In addition to the XRD experiments, some of the samples were analyzed by transmission electron microscopy (TEM), to determine if the stabilized ZrO_2 corresponded to the cubic or tetragonal phase. Fig. 3 shows the bright field image and electron diffraction pattern of the SDBS–NaOH sample. As it can be seen, the ZrO_2 particles are polyhedral particles with sizes no larger than 30–40 nm, which is in good agreement with the particle size limit described previously for the cubic and tetragonal constrainment stabilization ($\leq$ 50 nm). Additionally, the electron diffraction pattern recorded for that sample (inset of Fig. 3) had well-defined diffractions rings, which corroborated the nanocrystal formation. The distance of the diffraction rings fitted to the cubic lattice of ZrO_2 (JPCDS 01-089-969), which is in very good agreement with the previous reported about the Na-doped cubic ZrO_2 phase [9]. If the tetragonal ZrO_2 phases were present, the second diffraction electron ring must be a double ring, instead of the unique ring depicted. This result confirms the presence of the cubic ZrO_2 phase.

After the structural characterization, samples were microstructurally analyzed to elucidate if the surfactants influence and the presence of sodium hydroxide modify the ZrO_2 morphological or textural properties. Fig. 4 shows the N_2 adsorption–desorption isotherms of ZrO_2 samples prepared with different surfactants and with/without NaOH. All samples presented isotherms type II and IV, with their corresponding H3 and H2 hysteresis loops [33]. Samples composed by the monoclinic and cubic ZrO_2 mixtures presented isotherms type IV and H2 hysteresis. This kind of N_2 adsorption–desorption isotherms are associated to mesoporous materials. On the other hand, the Na-doped cubic ZrO_2 samples presented isotherms that corresponds to non-porous or macroporous powders, where the aggregates are not rigid. Fig. 5 presents the pore size distribution obtained using the BJH model [33]. CTAB and triton 114X samples presented a well defined unimodal pore size distribution of 2.1 and 1.6 nm, respectively. In contrast, sodium containing samples presented multimodal and not well defined pore size distributions, varying the pore size between 1.2 and 16.3 nm (see Table 1). Fig. 5A and 5B shows, as an example, the images of the sample synthesized with Triton 114X in the absence and presence of NaOH, respectively. The morphological influence due to an increase

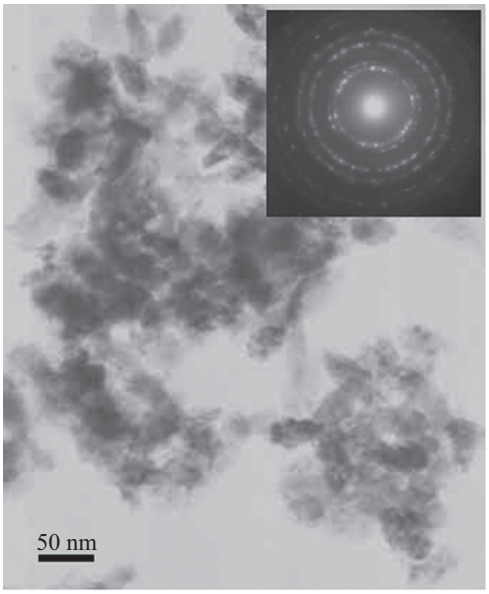

Fig. 3. Transmission electron bright field image and electron diffraction pattern (DBS–NaOH sample).

in the particle size of the sample synthesized with NaOH is observed. This morphological effect is examined in further detail below in Fig. 6. Thus, this is in good agreement with the N_2 adsorption isotherm type, which suggests that those samples does not contain defined porous. As it could be expected, the surface area and pore volume of these materials varied as well. CTAB and triton 114X samples presented the highest S_{BET} (67.0 m^2/g), while the other samples (non-porous) decreased the S_{BET}, up to 39.2 m^2/g (see Table 1).

It must be pointed out that between the cubic ZrO_2 samples (prepared in the presence of NaOH), the sample synthesized with a non-ionic surfactant (triton 114X) presented the best surface area. Finally, the pore volume grew inversely to the surface area, which suggests a porous sintering process. Therefore, there is a microstructural evolution as a function of the ZrO_2 phase composition. Initially, the monoclinic and cubic ZrO_2 mixtures posses some mesoporosity, which is destroyed when the cubic phase formation is induced, producing some dense and tiny nanoparticles (30–40 nm).

The microstructural characteristics of these samples were complemented by SEM (Fig. 6). As in the N_2 adsorption–desorption analysis, the samples presented two well defined morphologies. Samples prepared with CTAB or triton 114X, without the NaOH addition, produced large particles (>1 μm) with highly corrugated surfaces (Fig. 6A and 6B). Conversely, SDBS and all the NaOH containing samples presented a totally different morphology. In these cases, very tiny particles (30–80 nm) are agglomerated, producing macropore agglomerates larger than 1 μm (Fig. 6-C–F). In fact, the only significant difference among these samples is that the samples prepared with NaOH produced elongated particles,

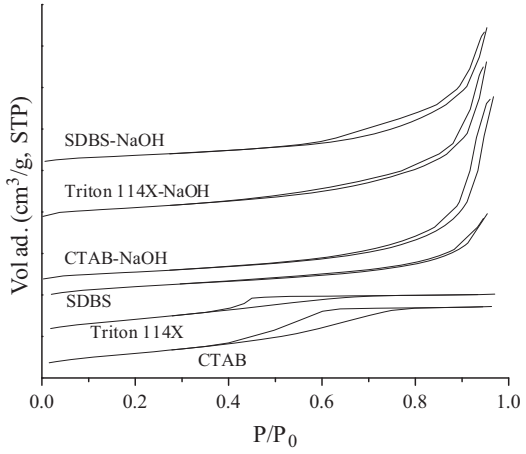

Fig. 4. N_2 adsorption–desorption isotherms of ZrO_2 samples prepared with different surfactants, in the absence or presence of NaOH. Curves were displaced over the *Y*-axis for a better visualization.

Table 1
Structural and microstructural data of all ZrO_2 samples prepared with different surfactants, in the absence or presence of NaOH.

Sample	Crystalline phase composition	S_{BET} (m^2/g)	Pore size (nm)	Pore volume (cm^3/g)
CTAB	Monoclinic+cubic	67.0	2.1	0.079
Triton 114X	Monoclinic+cubic	66.4	1.6	0.049
SDBS	Cubic	54.5	1.2–12.3	0.094
CTAB+NaOH	Cubic	41.8	4.1–16.3	0.205
Triton 114X+NaOH	Cubic	48.3	3.1–12.4	0.178
SDBS+NaOH	Cubic	39.2	4.0–13.1	0.154

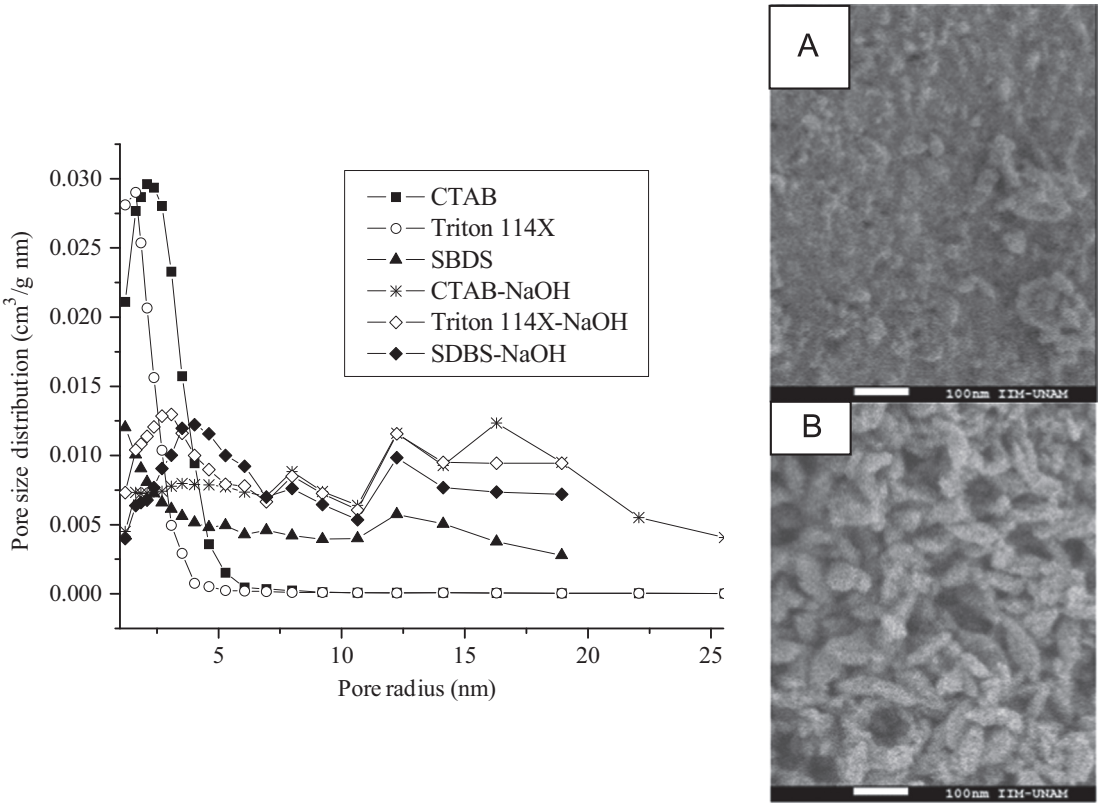

Fig. 5. Pore size distribution obtained by the BJH model for all ZrO_2 samples prepared with different surfactants, in the absence or presence of NaOH. (A) the SEM image of the sample synthesized with Triton 114 without NaOH and (B) the sample synthesized with NaOH.

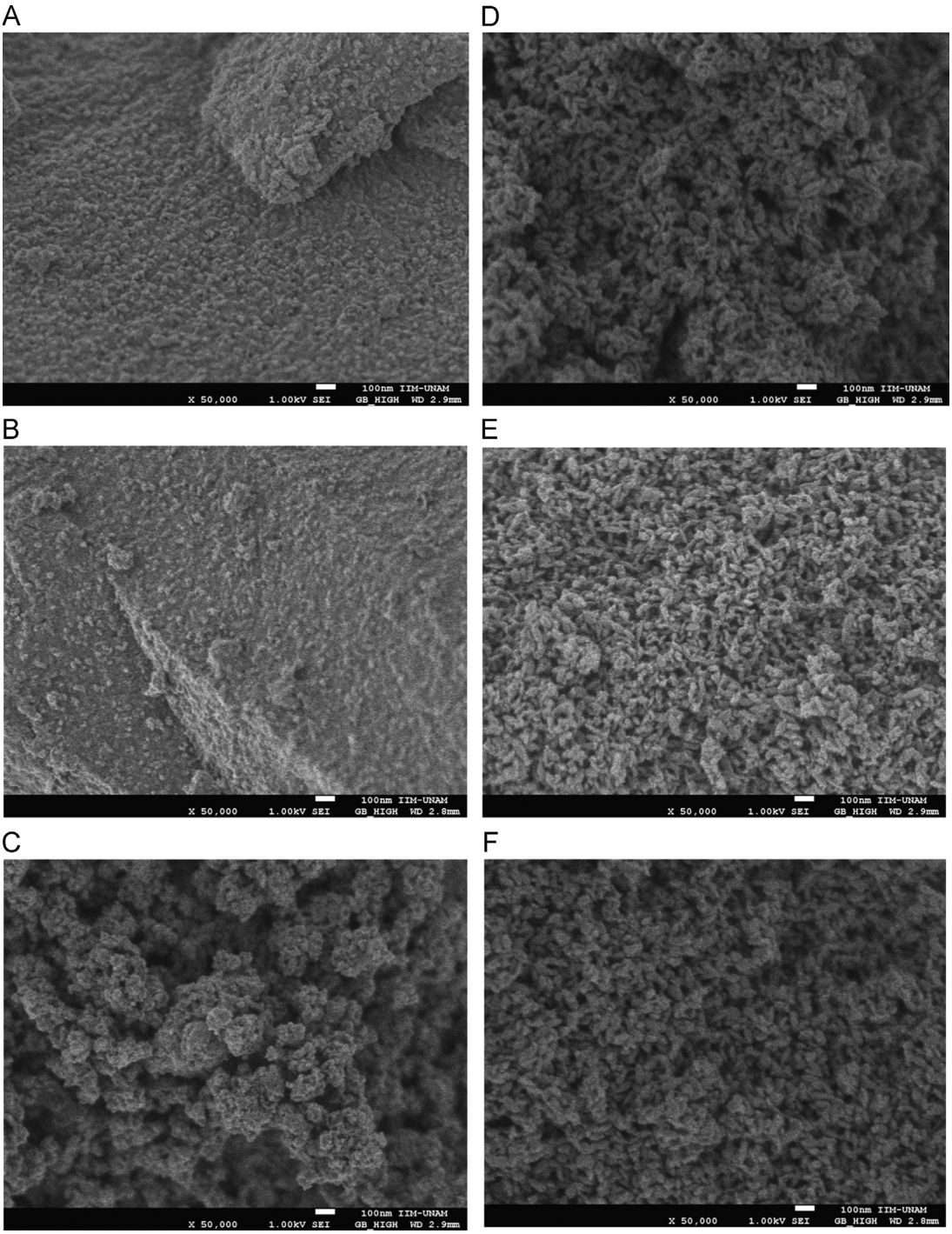

Fig. 6. Scanning electron images of all ZrO_2 samples prepared with different surfactants, in the absence or presence of NaOH: (A) CTAB, (B) triton 114X, (C) SDBS, (D) CTAB–NaOH, (E) triton 114X–NaOH and (F) SDBS–NaOH.

while the SDBS sample (without NaOH, Fig. 6C) produced particles which tend to be spherical.

ZrO_2 samples were hydrated with N_2 or CO_2 as gas carriers, in order to elucidate chemical variations on the surfaces due to the sodium effect. Fig. 7A shows the adsorption–desorption isotherms of the CTAB and SDBS samples, which varied in phase composition and surface area. Both isotherms were type III and the isotherms closed meaning that adsorption processes are reversible. Although both samples adsorb similar weights at around 80% of relative humidity (RH), it is evident that SDBS sample tended to increase its weight at lower RH than CTAB samples. SDBS sample has a smaller surface area. So, this effect may be attributed to the cubic phase or to the sodium present at the surface, which is a very hygroscopic element. Hence, to identify if the structural phase or the sodium effect produced the previous effects, different isotherms were obtained in the SDBS and SDBS–NaOH samples, using CO_2 or N_2 as gas carriers (Fig. 7B). Once again, isotherms were type III, but in this case the SDBS–NaOH isotherm did not totally close (in the CO_2 presence), indicating a partial irreversibility. This Na-doped cubic ZrO_2 sample must contain the highest sodium quantities, obtained from the SDBS and NaOH. However, the irreversible process was not observed when N_2 was used as gas carrier, although the maximum adsorption was similar at 80% of RH. Thus, the irreversible effect can be attributed to the sodium reactivity with

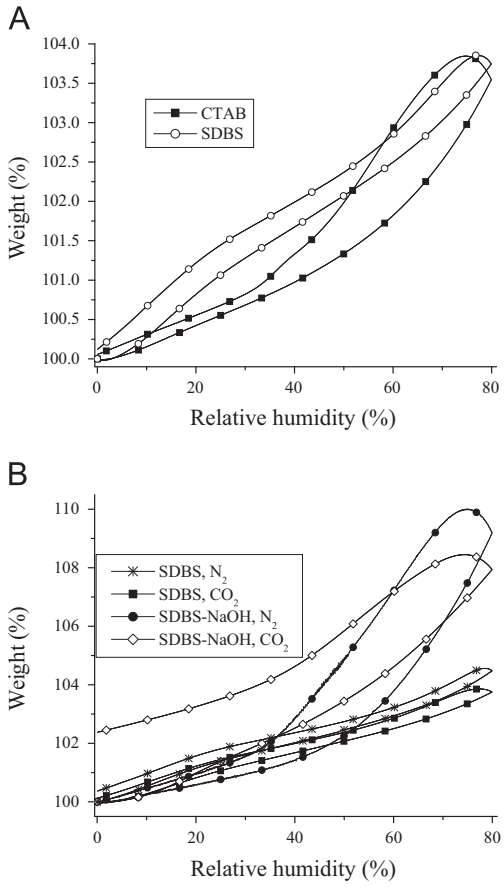

Fig. 7. Water sorption/desorption isotherms on the CTAB and SDBS samples using CO_2 as carrier gas (A). Water sorption/desorption isotherms on the SDBS and SDBS–NaOH samples using either N_2 or CO_2 as carrier gas (B). All isotherms were performed at 60 °C.

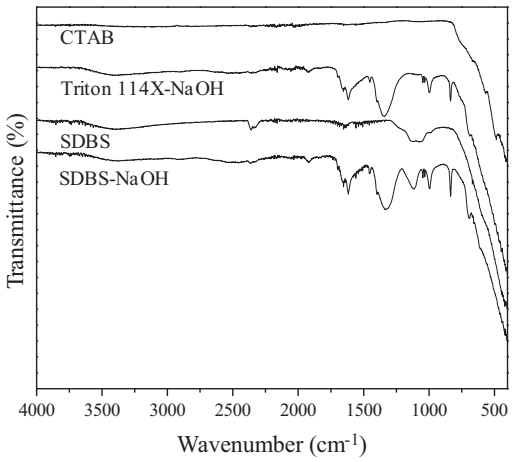

Fig. 8. ATR-FTIR spectra of different ZrO_2 samples prepared with different surfactants, in the absence or presence of NaOH.

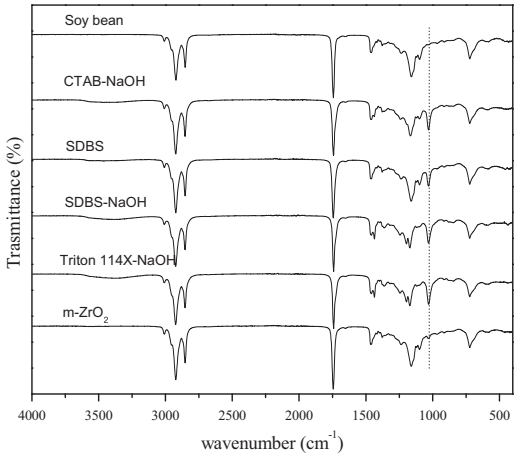

Fig. 9. ATR-FTIR spectra of soybean oil, various biodiesel products obtained with ZrO_2 samples prepared with different surfactants and monoclinic ZrO_2.

CO_2, producing Na–CO_3 superficial species (not necessarily crystalline sodium carbonate). In fact, when the SDBS sample, without NaOH, was subjected to the same experimental conditions, the adsorptions were considerably lower than in the CO_2 cases (only ~35% of efficiency in comparison to the NaOH containing samples). All these results indicate that adsorption process has significantly improved by the surface reactivity (sodium presence), but not by the crystalline structure, as both samples are Na-doped cubic ZrO_2.

Finally, ATR-FTIR of the CO_2–H_2O isotherm products were obtained to confirm the formation of hydroxyl and carbonate species, Fig. 8 shows some representative examples of them. Mixed monoclinic and cubic ZrO_2 sample-product, previously synthesized with CTAB, did not present any band vibration between 4000 and 830 cm^{-1}, only the metal-oxide (Zr–O) band vibrations were present at $< 800\ cm^{-1}$ [34–35]. Therefore, this ZrO_2 sample did not chemisorb water and/or CO_2 during the CO_2–H_2O isotherms, as it could be expected, because sodium was not present on it. In the cubic ZrO_2 sample, prepared with triton 114X and NaOH, there were observed several new vibration bands. Initially, between 3650 and 3000 cm^{-1} it can be observed a wide and tiny vibration band, which corresponds to the O–H vibration [34]. In addition, the following vibration bands appeared at 1922, 1650, 1619, 1456, 1342, 1045, 1025, 1000 and 835 cm^{-1}. All these vibration bands fitted with the sodium bicarbonate ($NaHCO_3$) FTIR spectrum [36–37]. Therefore, the sodium present in the sample reacted with CO_2 and H_2O to produce $NaHCO_3$. Sodium bicarbonate is thermally stable up to 100 °C, a higher temperature than that used on the CO_2–H_2O isotherms. Therefore, part of the NaOH present in the sample was used to stabilize the cubic ZrO_2 phase, and the rest must have stayed at the surface, reacting later with CO_2 and H_2O. In fact, this idea is supported by the ATR-FTIR spectra of both SDBS samples, without and with NaOH. The sample without NaOH practically did not produce $NaHCO_3$, as most of the sodium must be into the ZrO_2 structure, stabilizing the cubic phase. On the contrary, the SDBS sample synthesized with NaOH, clearly showed the $NaHCO_3$ vibrations bands. These results are in good agreement with the fact that it was the unique sample that during the CO_2–H_2O isotherms presented a weight increment, attributed to the gained CO_2 and H_2O. Finally, it has to be mentioned that both SDBS samples presented an additional vibration band at 1122 cm^{-1}, corresponding to the residual SDBS present in the sample.

In addition, for testing the basic catalytic activity of samples the transesterification reaction was performed for biodiesel production. Fig. 9 shows the ATR-FTIR spectra of the biodiesel produced at 3 h and 65 °C using different ZrO_2 samples. Although the spectra do not exhibit any major changes, there are some specific vibration bands that identify the biodiesel production: 2972, 1741, and 1188 cm^{-1}. At approximately 3330 cm^{-1}, there is a wide vibration band associated with O–H bonds that corresponds to the presence of non-reacted methanol [37]. The O–H vibration band can be only observed in the biodiesels produced with the ZrO_2 samples prepared with surfactant but without NaOH, indicating an

Table 2
Biodiesel yields obtained from the different catalysts.

Sample	Yield (%)	Density (g/mL)
CTAB	–	–
Triton 114X	–	–
SDBS	86	0.89
CTAB+NaOH	93	0.87
Triton 114X+NaOH	93	0.86
SDBS+NaOH	93	0.86
m-ZrO_2	–	–

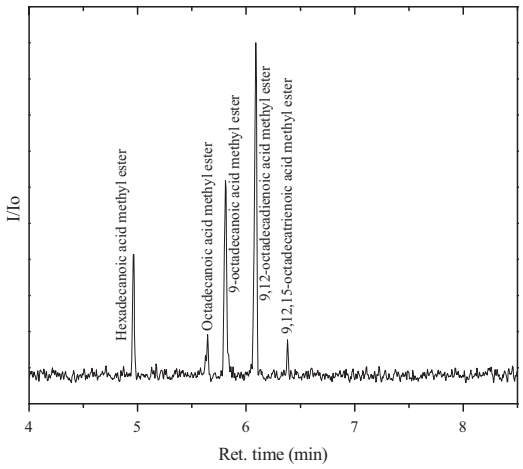

Fig. 10. Representative gas chromatogram obtained from the biodiesel produced of different ZrO_2 samples prepared with different surfactants in presence of NaOH.

incomplete reaction. In fact the biodiesel conversion in these samples was considerably low. However, all samples containing sodium, from the synthesis method, presented high yield, ~93%. The presence of a strong C=O double bond band at ~1740 cm^{-1} corresponds to the carbonyl radical and it is characteristic of the ester group, which confirms the transesterification of the soybean oil [38]. In addition, the band located at 1450 cm^{-1} corresponds to the asymmetric stretching of the C–H bond and the asymmetric bending of the functional group (–CH_3 antisymmetric vibrations). There is a set of bands between 1000 and 1300 cm^{-1} that are associated with asymmetric vibrations of the C–C(=O)–O and O–C–C bonds. The high intensity bands located at 1200 cm^{-1} are attributed to the stretching of the methyl group O–CH_3 and to the axially asymmetric deformation of the C–C=O bonds. The bands between 1100–1170 cm^{-1} correspond to the vibrations of the C–CH_2–O group, the asymmetric stretching of C–O–C and C–C bond stretching. The band located at ~1000 cm^{-1} is attributed to the symmetric angular deformation of the C–H bond of olefins. The methylene group presents scissors vibrations at 1463 and torsion vibrations at 721 cm^{-1}, respectively [39]. It should be noted that all samples with sodium exhibit only cubic phase composition (see Table 1). However, the samples synthesized without sodium did not produced biodiesel. It may be related to the ZrO_2 has weak acid and base sites on the surface that modified the reactivity. Table 2 summarizes the biodiesel yields of the different catalysts as a function of the Na presence. The yields obtained for the CTAB, Triton 114X and SDBS with NaOH render ~93%. The density values are in concordance with the ASTM-D1298 norm (0.86–0.90 g/mL).

The biodiesels were finally characterized using a GC–MS analysis to elucidate their chemical compositions. Fig. 10 shows a typical chromatogram obtained from the biodiesel product catalyzed by ZrO_2 in the presence of SBDS-Na. All samples have similar chromatograms with 5 similar FAME (fatty acid methyl ester) retention times. The first well-defined peak observed at 5.1 min corresponds to the hexadecanoic acid methyl ester (CH_3–O–CO–$(CH_2)_{14}$–CH_3, methyl palmitate). The second peak, at 5.8 min, was associated with octadecanoic acid methyl ester (CH_3–O–CO–$(CH_2)_{16}$–CH_3, methyl stearate). Then, the unsaturated molecules were associated to three peaks that appear at 6.0, 6.25 and 6.55 min. The peak at 6.0 is associated to 9-octadecanoic acid methyl ester (CH_3–O–CO–$(CH_2)_7$–CH=CH–$(CH_2)_7$–CH_3). At 6.25 min, the retention time corresponds to 9,12-octadecadienoic acid methyl ester (CH_3–O–CO–$(CH_2)_7$–CH=CH–CH_2–CH=CH–$(CH_2)_4$–CH_3) and the last peak at 6.55 min was assigned to 9,12,15-octadecatrienoic acid methyl ester (CH_3–O–CO–$(CH_2)_7$–CH=CH–CH_2–CH=CH–CH_2–CH=CH–CH_2–CH_3). In addition, the chemical compositions of these peaks were identified by mass spectrometry, which showed that these were a typical mixture of biodiesel esters. The mass values correspond to 270, 298, 296, 294 and 292 *m*/*z* to the respective methyl esters and its retention times. Results evidenced that basic catalytic activity strongly depends on the sodium addition during the hydrothermal ZrO_2 synthesis.

4. Conclusions

Different nano-crystalline ZrO_2 samples were successfully synthesized via a simple hydrothermal method in the presence of various surfactants (cationic, non-ionic and anionic) and sodium hydroxide. Initially, XRD and TEM results showed that samples prepared with CTAB and triton 114X, as surfactants, produced a mixture of monoclinic and cubic ZrO_2 phases. Here, the formation of the cubic ZrO_2 phase was explained in terms of a constrainment mechanism. On the other hand, if SDBS was used as surfactant, the final powder was pure cubic ZrO_2. In this case, the cubic ZrO_2 phase was stabilized by a Na-doping process, with the sodium coming from the SDBS surfactant. This hypothesis was conformed by new synthesis with CTAB and triton 114X, where NaOH was added. The XRD patterns of these new samples only showed the production of cubic ZrO_2 phase.

The microstructural characteristics of the different samples were analyzed by N_2 adsorption–desorption and SEM. While the monoclinic-cubic ZrO_2 samples presented a well defined mesoporosity and the highest surface area, cubic ZrO_2 samples decreased their surface area, and the porosity tended to disappear. Additionally, the scanning electron microscopy characterization revealed the formation of agglomerated nano-particles. Therefore, surfactant and sodium additions played important roles to control structure and microstructure, resulting in the formation of different crystalline phases with some specific microstructural variations, as the surface area increase. There are no reports of this type of synthesis, morphological changes in products and their reactivity evaluation in applications as transesterification catalysis. Different CO_2–H_2O adsorption experiments were performed, showing that the powder surfaces changed their reactivity as a function of the sodium content, but not from the ZrO_2 crystalline structure. Finally, the sodium acts as an efficient cubic phase stabilizer. Therefore, the samples of cubic ZrO_2 phase synthesized with sodium present high activity to produce biodiesel with considerable yield about 93%.

Acknowledgments

The present work was financially supported by the project IN102313 PAPIIT-UNAM. Authors thank to Adriana Tejeda, Carlos Flores and Omar Novelo for technical help.

References

[1] J. Ortiz-Landeros, M.E. Contreras-García, H. Pfeiffer, J. Porous Mater 16 (2009) 473–479.
[2] W. Jung, J.L. Hertz, H.L. Tuller, Acta Mater. 57 (2009) 1399–1404.
[3] F.C. Fonseca, D.Z. de Florio, R. Muccillo, Solid State Ionics 180 (2009) 822–826.
[4] L.A. Diaz-Torres, E. de la Rosa, P. Salas, V.H. Romero, C. Angeles-Chavez, J. Solid State Chem. 181 (2008) 75–80.
[5] G. Larsen, E. Lotero, L.M. Petkovic, D.S. Shobe, J. Catal. 169 (1997) 67–75.
[6] C. Zhang, C. Li, J. Yang, Z. Cheng, Z. Hou, Y. Fan, J. Lin, Lang 25 (2009) 7078–7083.
[7] C.H. Wu, S.Y. Chen, P. Shen, J. Solid State Chem. 200 (2013) 170–178.
[8] C. Gionco, M.C. Paganini, E. Giamello, R. Burgess, C. Di Valentin, G. Pacchioni, J. Phys. Chem. Lett. 5 (2014) 447-451.
[9] H. Näfe, N. Karpukhina, J. Am. Ceram. Soc. 90 (2007) 1597–1602.
[10] C. Cau, Y. Guari, T. Chave, J. Larionova, P. Pochon, S.I. Nikitenko, J. Phys. Chem. C 117 (2013) 22827–22833.
[11] F. Monte, W. Larsen, J.D. Mackenzie, J. Am. Ceram. Soc. 83 (2000) 628–634.
[12] D.G. Lamas, A.M. Rosso, M. Suarez, A. Fernández, M.G. Bellino, M.D. Cabezas, N.E. Walsöe de Reca, A.F. Craievich, Scripta. Mater. 55 (2006) 553–556.
[13] Y. Murase, E. Kato, K. Daimon, J. Am. Ceram. Soc. 69 (1986) 83–87.
[14] J. Wang, R. Raj, J. Am. Ceram. Soc. 74 (1991) 1707–1709.
[15] V.M. Shinde, G. Madras, Inter. J. Hydrogen Energy 38 (2013) 13961–13973.
[16] M.K. Lam, K.T. Lee, A.R. Mohamed, Biotech. Adv. 28 (2010) 500–518.
[17] Y. Li, B. Ye, J. Shen, Z. Tian, L. Wang, L. Zhu, T. Ma, D. Yang, F. Qiu, Biores. Tech. 137 (2013) 220–225.
[18] J. Ortiz-Landeros, M.E. Contreras-García, C. Gómez-Yáñez, H. Pfeiffer, J. Solid State Chem. 184 (2011) 1304–1311.
[19] K. Byrappa, T. Adschiri, Prog. Cryst. Growth Char. Mater. 53 (2007) 117–166.
[20] X. Liang, R.L. Patel, Ceram. Int. 40 (2014) 3097–3103.
[21] C. Bluthardt, C. Fink, K. Flick, A. Hagemeyer, M. Schichter, A. Volpe Jr., Catal. Today 137 (2008) 132–143.
[22] F. Prete, A. Ruzzuti, L. Esposito, A. Tucci, C. Leonelli, J. Am. Ceram. Soc. 94 (2011) 3587–3590.
[23] F. Khan, M. Eswaramoorthy, C.N.R. Rao, Solid State Sci. 9 (2007) 27–31.
[24] N.A. Turta, P. De Luca, N. Bilba, J.B. Nagy, A. Nastro, Micropor. Mesopor. Mater. 112 (2008) 425–431.
[25] S. Wang, H. Xiu, L. Qian, X. Jia, J. Wang, Y. Liu, W. Tang, J. Solid State Chem. 182 (2009) 1088–1093.
[26] B. Lu, Y.S. Lin, J. Mater. Sci. 46 (2011) 7056–7066.
[27] Y. Wang, A. Zhou, Z. Yang, Mater. Lett. 62 (2008) 1930–1932.
[28] S. Liu, O.I. Lebedev, M. Mertens, V. Meynen, P. Cool, G. van-Tendeloo, E.F. Vansant, Micropor. Mesopor. Mater. 116 (2008) 141–146.
[29] T. Caillot, Z. Salama, N. Chanut, F.J. Cadete, S. Aires, S. Bennici, A. Auroux, J. Solid State Chem. 203 (2013) 79–85.
[30] T. Gu, P.A. Galera-Gómez, Colloid. Surf. A: Physicochem. Eng. Aspects 104 (1995) 307–312.
[31] C. Vautier-Giongo, H.O. Pastore, J. Colloid Interface Sci. 299 (2006) 874–882.
[32] A.H. Saiyad, S.G.T. Bath, A.K. Rakshit, Colloid Polym. Sci. 276 (1998) 913–919.
[33] S. Lowell, J.E. Shields, M.A. Thomas, M. Thommes, Characterization of Porous Solids and Powders: Surface Area, Pore Size and Density, Kluwer Academic Publishers, London, 2004.
[34] K. Nakamoto, Infrared and Raman Spectra of Inorganic and Coordination Compounds, Wiley, USA, 2009.
[35] R.A. Nyquist, R.O. Kagel, Handbook of Infrared and Raman Spectra of Organic Compounds and Organic Salts, vol. 4, Academic Press Inc., New York, 1996.
[36] T. Hatakeyama, L. Zhenhai, Handbook of Thermal Analysis, Wiley, USA, 1998.
[37] G.G. Santilla-Reyes, H. Pfeiffer, J. Inter., Greenhouse Gas Control 5 (2011) 1624–1629.
[38] B. Salamatinia, A.Z. Abdullah, S. Bhatia, Fuel Proc. Technol. 97 (2012) 1–8.
[39] N.G. Siatis, A.C. Kimabari, C.S. Pappas, P.A. Tarantilis, M.G. Polissiou, J. Am. Oil Chem. Soc. 83 (2006) 53–57.